



Optics Letters

Passive laser power stabilization in a broadband noise spectrum via a second-harmonic generator

NANJING JIAO,^{1,†} RUIXIN LI,^{1,†} BINGNAN AN,¹  JIAWEI WANG,¹ LIRONG CHEN,^{1,2} YAJUN WANG,^{1,2,*}  AND YAOHUI ZHENG^{1,2,3} 

¹State Key Laboratory of Quantum Optics and Quantum Optics Devices, Institute of Opto-Electronics, Shanxi University, Taiyuan 030006, China

²Collaborative Innovation Center of Extreme Optics, Shanxi University, Taiyuan, Shanxi 030006, China

³yhzheng@sxu.edu.cn

[†]These authors contributed equally to this Letter.

*YJWangsxu@sxu.edu.cn

Received 18 March 2024; revised 17 May 2024; accepted 24 May 2024; posted 24 May 2024; published 18 June 2024

An extremely conspicuous passive power noise stabilization is the first, to the best of our knowledge, discovered in a cavity-enhanced second-harmonic generation (SHG) process. Differing from the SHG as a buffer reservoir, the stronger strength of the nonlinear interaction pushes the power noise suppression level to a higher value and exhibits a broadband noise reduction performance due to the mechanism of dynamic pump suppression in the SHG process. The noise is suppressed to near shot noise limit (SNL) among the kHz to MHz frequency range, accompanied by a maximum noise reduction of 35 dB. A comprehensive demonstration indicates that the nonlinear interaction has no function on the phase noise of fundamental and harmonic waves. A theoretical model is also established that is consistent well with the experimental results. The methodology is beneficial to multiple optical metrology experiments. © 2024 Optica Publishing Group

<https://doi.org/10.1364/OL.524119>

Due to inherent narrow linewidth, excellent beam quality, low power noise, and high stability, continuous-wave (CW) single-frequency laser has been widely applied to quantum precision measurement [1,2], quantum state preparation [3,4], gravitational wave detection [5–7], quantum information [8,9], biological imaging [10–12], etc. However, a free-running laser still suffers from a broadband power fluctuation, especially in the audio frequency band [13]. For instance, in the generation of a bright squeezed state at audio frequency, power noise above the shot noise limit (SNL) will impede the squeezing operation [4,14]. To meet the requirements of low-frequency applications in high-precision and highly sensitive measurements, various active [15–17] and passive [18–23] power noise stabilization schemes had been proposed to reduce the excess noise above SNL.

Compared with the active power noise stabilization, the passive scheme is not confined by the detectable power of the photodetector and feedback control loop gain and bandwidth. An optical cavity can be treated as an optical low-pass filter [24]. Then the transmission noise above the cavity linewidth is passively filtered. For a noise reduction in the audio frequency

band, a narrow linewidth (<1 kHz) ultra-stable cavity should be designed [20,21], albeit at the expense of increased experimental complexity and cost, as well as reduced power transmittance. A semiconductor optical amplifier (SOA) also acts as a noise reducer spectrum slicing source, in which a saturation gain had been utilized to suppress the power noise above 40 kHz [23]. SOA, incorporating with an active feedback control loop, had been proposed to suppress the power noise of 0.5 mW to near SNL, in the frequency range from 0.8 kHz to 50 MHz [25]. However, limited by the maximum injection power of the SOA, this method is only suited to a power noise reduction of a low power seed laser (~mW). In 2009, a strong noise reduction by more than 32 dB was reported by means of an off-resonant Kerr nonlinear cavity. However, additional noise at intermediate frequencies (1.5–9 MHz) increased with the increasing Kerr effect and probably internal Brillouin scattering [26]. In 2015, a second-harmonic generation (SHG) at very low conversion efficiency (<0.1%) was utilized as a buffer reservoir, which breaks the exclusive interaction between population inversion and photon population without modifying the static characteristics of the laser. It can mitigate about 20 dB excess noise lying at the laser relaxation oscillation (RO) of a solid-state laser [18]. In 2022, a passive laser power stabilization via an optical spring was proposed with a noise reduction range from 400 Hz to 100 kHz. They demonstrated that the relative power noise of the laser is stabilized from about $2 \times 10^{-5} \text{ Hz}^{-1/2}$ to a minimum value of $1.6 \times 10^{-7} \text{ Hz}^{-1/2}$, corresponding to the power noise reduction by a factor of 125 [19].

In this Letter, we report a passive power noise stabilization technology with a broadband spectrum and significant noise reduction, which has no impact on the phase noise. The strong noise reduction occurs in a cavity-enhanced SHG, and theoretical and experimental demonstrations co-point out that the power noise of the reflected fundamental wave is related to the conversion efficiency of the SHG. By optimizing the conversion efficiency to 70%, the maximum noise suppression of 35 dB is realized. It also presents a near SNL noise characteristic among the frequency range of 1 kHz–1 MHz. The extremely conspicuous performance of the noise stabilization owes to the mechanism of dynamic pump suppression in the

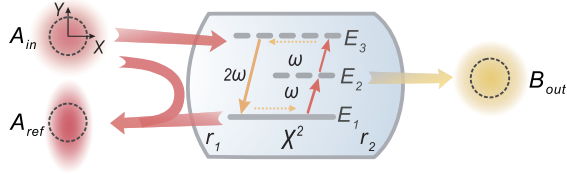


Fig. 1. Conceptual model for the noise transferring from a SHG cavity.

SHG process. The methodology is benefit to multiple optical metrology experiments.

Our passive power noise stabilization mechanism of the SHG is depicted as a three-step recycling process [27–31] in Fig. 1. The SHG shows how the presence of a field at frequency ω stimulates the upward electronic transition to generate a 2ω field [32]. An electron absorbs two photons of ω , and transits to the electronic excited state E3, whereafter comes back to the initial ground state E1, and spontaneously emits a photon of 2ω . With continuous pumping, the three-step electronic transition forms a regular recycling of the laser electronics, and a noise suppression of the pump source is established [27–31]. We focus on a cavity-enhanced SHG process, and its noise evolution can be expressed as the motion equations [32–34]. Under the boundary conditions of the SHG cavity, the quadrature power and phase noise variance of its reflected fundamental and second-harmonic waves can be deduced as [33,34]

$$V_{A,ref} = \frac{((\gamma_{in} - \gamma_{loss} - 3\mu\alpha^2)^2 + (2\pi\Omega)^2)V_{A,X_{in}} + 4\gamma_{in}\gamma_{loss}V_{loss} + 8\mu\alpha^2\gamma_{in}V_{B,X_{in}}}{(\gamma + 3\mu\alpha^2)^2 + (2\pi\Omega)^2}, \quad (1)$$

$$V_{A,refphase} = \frac{((\gamma_{in} - \gamma_{loss} + \mu\alpha^2)^2 + (2\pi\Omega)^2)V_{A,Y_{in}} + 4\gamma_{in}\gamma_{loss}V_{loss} + 8\mu\alpha^2\gamma_{in}V_{B,Y_{in}}}{(\gamma + \mu\alpha^2)^2 + (2\pi\Omega)^2}, \quad (2)$$

$$V_{B,out} = \frac{((- \gamma + \mu\alpha^2)^2 + (2\pi\Omega)^2)V_{B,X_{in}} + 8\mu\alpha^2\gamma_{loss}V_{loss} + 8\mu\alpha^2\gamma_{in}V_{A,X_{in}}}{(\gamma + 3\mu\alpha^2)^2 + (2\pi\Omega)^2}, \quad (3)$$

$$V_{B,outphase} = \frac{((- \gamma + 3\mu\alpha^2)^2 + (2\pi\Omega)^2)V_{B,Y_{in}} + 8\mu\alpha^2\gamma_{loss}V_{loss} + 8\mu\alpha^2\gamma_{in}V_{A,Y_{in}}}{(\gamma + \mu\alpha^2)^2 + (2\pi\Omega)^2}, \quad (4)$$

where $V_{A,X_{in}}$ and $V_{A,Y_{in}}$ are the power and phase noise variance of the injected fundamental wave with a power of P_{in} , respectively. If the input of the second-harmonic wave $V_{B,X_{in}}$, $V_{B,Y_{in}}$ and the leakage of the fundamental wave V_{loss} are minimum-uncertainty states, then $V_{A,loss} = V_{B,X_{in}} = V_{B,Y_{in}} = 1$, defines $V=1$ as the SNL according to the mode operator. Ω is the analysis frequency. $\gamma = \gamma_{in} + \gamma_{out} + \gamma_{loss}$ is the overall cavity photon loss rate at the fundamental wave, and the rates of the input coupler γ_{in} , the output coupler γ_{out} , and the intracavity photon loss γ_{loss} are determined by the experimental measurement and theory.

The semiclassical steady-state solutions of the fundamental cavity mode operator α , the circulating power P_{circ} , and the two-photon damping rate μ are expressed as [34]

$$\alpha = \frac{\sqrt{2\gamma_{in}}A_{in}}{\gamma_{in} + \mu\alpha^2}, \quad (5)$$

$$P_{circ} = \frac{|\alpha|^2 \hbar\omega}{\tau}, \quad (6)$$

$$\mu = \frac{\hbar\omega}{2\tau^2} \frac{16d_{eff}^2 \hbar\pi^2 l}{\lambda^3 n_1 n_2 \epsilon_0 c}. \quad (7)$$

α is extracted from $P_{in} = \hbar\omega A_{in}^2$. A_{in} is associated with the incident power, and $\hbar\omega$ is the photon energy. The circulating power P_{circ} is related to α . The two-photon damping rate depends on the nonlinear interaction strength of the nonlinear crystal and the geometrical parameters of the resonator, which represents the nonlinear loss from the conversion of the fundamental wave to the second-harmonic wave. d_{eff} and l are the effective nonlinear coefficient and length of the crystal, respectively. h is the B–K focusing factor. λ is the wavelength of the fundamental wave. n_1 and n_2 are the refractive indices of the fundamental and second-harmonic waves, respectively. ϵ_0 is the permittivity in free space, and c is the vacuum speed of light. $\tau = 2L_0/c$ is the round trip time of the fundamental wave in the cavity. L_0 is the optical length of the cavity.

Figure 2 shows a simplified schematic for the quadrature noise suppression and calibration of the SHG process. The laser source is a 2 W CW single-frequency 1550 nm fiber laser (NKT, Koheras BASIK X15). Its output passes through a Faraday isolator (FI), an electro-optical modulator (EOM) [35], and a dichroic beam splitter (DBS) and then is injected into the SHG. The SHG is a semi-monolithic cavity consisting of a concave mirror driven by a piezoceramics and a periodically poled KTiOPO₄ (PPKTP) crystal (10 mm × 2 mm × 1 mm) [36,37]. The curvature radius of the convex surface of the crystal is 12 mm, which is high reflected (HR) for both 1550 nm and 775 nm wavelengths, and its plane front face is coated as anti-reflectivity (AR) for both wavelengths. The output coupler is a concave mirror with a radius of

the curvature of 30 mm and has a transmissivity of $12 \pm 1.5\%$ for 1550 nm and high transmissivity (HT) for 775 nm. The linewidth of the SHG cavity is 68 MHz corresponding to an air

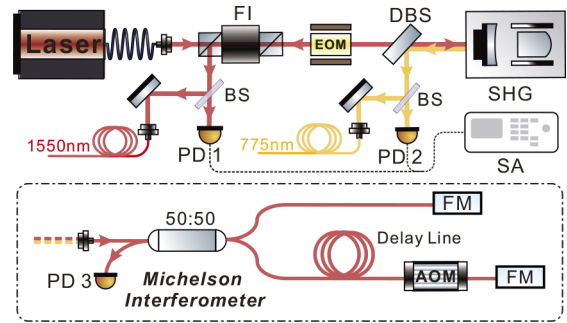


Fig. 2. Experimental setup of the power noise stabilization, power, and phase noise measurement. FI, Faraday isolator; EOM, electro-optical modulator; SHG, second-harmonic generator; DBS, dichroic beam splitter; BS, beam splitter; 50:50, 50:50 fiber-optic coupler; PD, photodetector; AOM, acousto-optic modulator; FM, Faraday mirror; SA, spectrum analyzer.

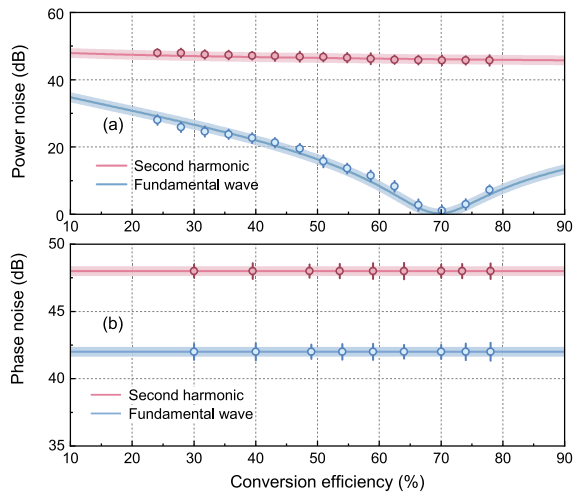


Fig. 3. Normalized power and phase noise of the second-harmonic and reflected fundamental waves at the analysis frequency of 500 kHz and the detected power of 1 mW versus the SHG conversion efficiency. The theoretical fitting curve and experimental results of the (a) power noise and (b) phase noise.

gap of 27 mm. The DBS is used to separate the second-harmonic wave from the fundamental one.

The fundamental wave reflected by the SHG is separated by the FI, and the generated second-harmonic one is directly reflected by the DBS. Both waves are divided into two parts. One is used for power noise measurement (photodetector 1/2, (PD1/2), New Focus, Models2053), and the other is injected into an all-fiber non-equilibrium Michelson interferometer for phase noise calibration. The coupling ratio of the fiber coupler in the interferometer is 50:50, and the lengths of the two arms are 1 m and 101 m, respectively. Two Faraday mirrors (FMs) are employed to compensate the birefringent effect-induced polarization degeneration and maintain the maximum beat signal amplitude between the two fibers. An acoustic-optic modulator (AOM SGTF40-1550-1T-2A1) with a frequency shift of 40 MHz is installed in the 101 m arm, and the same AOM and fiber are applied for a phase noise calibration of 775 nm. The beat signal at 80 MHz is detected by PD3 and then is demodulated to extract the phase noise.

To demonstrate the overall perspective of the noise evolution characteristic in the SHG process, we measure the phase and power noises of the reflected fundamental and generated second-harmonic waves with the scheme in Fig. 2, and the noise characteristics under different frequency doubling conversion efficiency are shown in Fig. 3 at the analysis frequency of 500 kHz. All the measurements are carried out with a detected power of 1 mW, and we carefully calibrate the conversion efficiency and detected power several times for each measurement. The conversion efficiency is manipulated by changing the input power of the SHG. The results demonstrate that the power noise of the second-harmonic wave exhibits minimal variation with the increase of the conversion efficiency. However,

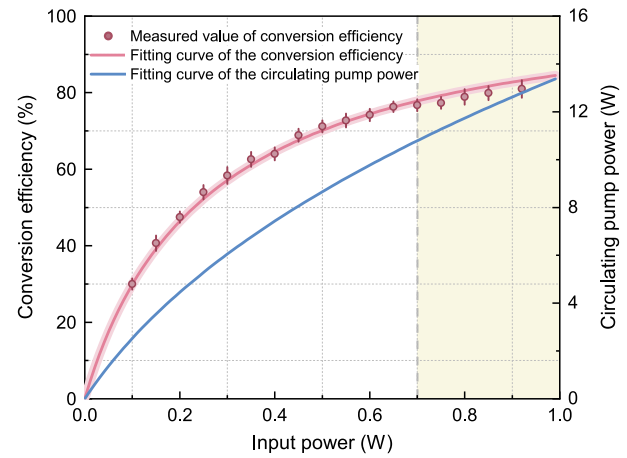


Fig. 4. Evolution of conversion efficiency and circulating pump power with input power.

the reflected fundamental one presents a power noise reduction phenomenon, and the noise power is reduced to the lowest level at 70% conversion efficiency, corresponding to a 35 dB noise reduction compared with the free-running laser. At this point, the reflected available fundamental wave power is 112 mW, and only 1 mW is separated for noise characteristic analysis. With increasing conversion efficiency further, the noise grows up to a higher level. Simultaneously, the phase noise of the two beams holds constant under different conversion efficiency. The experimental results are also theoretically simulated by Eqs. (1)–(4) with the detailed parameters in Table 1. The theoretical analysis is consistent well with the experimental one. It indicates that the nonlinear interaction in the SHG only modifies the power noise of the reflected fundamental wave and has no influence on the phase noise of the two waves.

Figure 4 presents the conversion efficiency and circulating pump power of the SHG. With the increase of the input/pump power, the conversion efficiency steadily rises to represent a quick boosting of the electronic transition between E1 and E3, meanwhile strengthening the two-photon transition to form a stronger recycling of the laser electronics, in which more power noise suppression is realized for the pump field. By comparing the analysis data in Fig. 3 and Fig. 4 with Eq. (1), the nonlinear interaction strength $3\mu\alpha^2$ is the main influence factor for our passive noise stabilization technology, and the optimum power noise suppression is realized at $\gamma_{in} = \gamma_{loss} + 3\mu\alpha^2$. In this case, a steady state of the closed excitation cycle is established (Fig. 1), in which the decay rate of the injected photons equals to the sum of the single-photon and two-photon loss rates. After the inflection point of 70%, the conversion efficiency verges to slowly changing status and becomes flattened out after this point. Under the circumstances, a stronger nonlinear interaction $3\mu\alpha^2$ prompts $\gamma_{in}\gamma_{loss} + 3\mu\alpha^2$ and raises the power noise of the pump laser. Simultaneously, the circulating power variation trend shows no change in this area. By continuously increasing the input power,

Table 1. Detailed Parameters of the SHG Cavity in the Simulation

Parameter	d_{eff}	h	l	n_1	n_2	ϵ_0	c	L_0	$V_{A,Xin}$
Value	10.8 pm/V	1.25	10×10^{-3} m	1.8158	1.8461	8.85×10^{-12}	3×10^8 m/s	7.8×10^{-2} m	35 dB

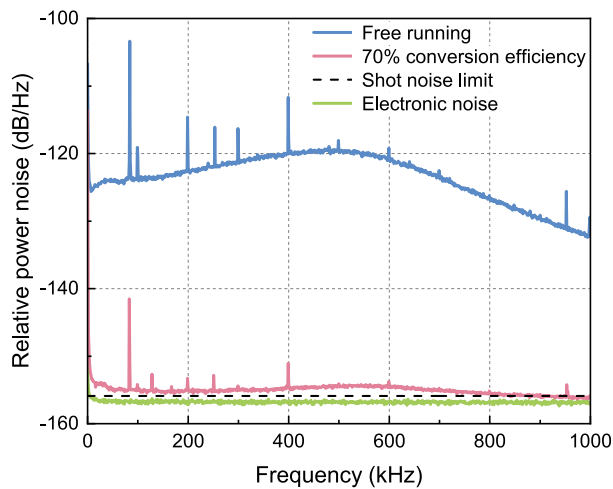


Fig. 5. Broadband power noise spectrum of the reflected fundamental wave at the conversion efficiency of 70%. Resolution bandwidth (RBW), 100 Hz, and video bandwidth (VBW), 10 Hz.

the excess noise of the pump laser degrades the noise suppression effect. These two factors create a bottleneck for this passive power noise stabilization technology. A broadband power noise spectrum among kHz to MHz is also collected as shown in Fig. 5 with a detected power of 1 mW at the conversion efficiency of 70%. Compared with the free-running power noise, the maximum noise suppression is up to 35 dB (from -120 to -155 dB/Hz). The ultimate noise level approaches the SNL from 1 to 800 kHz and reaches the SNL beyond 800 kHz. Here, we omit the measured results beyond 1 MHz, and the poor performance of the detector below 1 kHz limits the low-frequency measurement to 1 kHz.

An extremely conspicuous passive power noise stabilization is firstly discovered in a cavity-enhanced SHG process. The power noise of a 1550 nm fiber laser is suppressed to near SNL across a frequency range from kHz to MHz, and a maximum noise reduction of 35 dB was demonstrated from -120 to -155 dB/Hz. The noise reduction is related to the strength of the nonlinear interaction in the SHG process and has no impact on the phase noise of the fundamental and harmonic waves. The main physical mechanism of this effect is demonstrated to be the three-step recycling process of electronic transition in the SHG. The theoretical analysis is consistent well with the experimental results. The methodology can be applied to multiple optical metrology experiments.

Funding. National Natural Science Foundation of China (62225504, 62027821, 62375162, U22A6003); National Key Research and Development Program of China (2020YFC2200402).

Disclosures. The authors declare no conflicts of interest.

Data availability. Data underlying the results presented in this paper are not publicly available at this time but may be obtained from the authors upon reasonable request.

REFERENCES

- W. Huang, X. Liang, B. Zhu, *et al.*, *Phys. Rev. Lett.* **130**, 073601 (2023).
- X. Sun, W. Li, Y. Tian, *et al.*, *Photonics Res.* **10**, 2886 (2022).
- W. Yang, S. Shi, Y. Wang, *et al.*, *Opt. Lett.* **42**, 4553 (2017).
- F. Meylahn, B. Willke, and H. Vahlbruch, *Phys. Rev. Lett.* **129**, 121103 (2022).
- A. Perreca, A. F. Brooks, J. W. Richardson, *et al.*, *Phys. Rev. D* **101**, 102005 (2020).
- A. Buikema, C. Cahillane, G. Mansell, *et al.*, *Phys. Rev. D* **102**, 062003 (2020).
- L. Barsotti, J. Harms, and R. Schnabel, *Rep. Prog. Phys.* **82**, 016905 (2019).
- S. Shi, L. Tian, Y. Wang, *et al.*, *Phys. Rev. Lett.* **125**, 070502 (2020).
- S. Shi, Y. Wang, L. Tian, *et al.*, *Laser Photonics Rev.* **17**, 2200508 (2023).
- M. Münter, M. Pieper, T. Kohlfaerber, *et al.*, *Biomed. Opt. Express* **12**, 6024 (2021).
- A. M. Kho and V. J. Srinivasan, *Opt. Express* **29**, 42037 (2021).
- K. Hashimoto, J. Omachi, and T. Ideguchi, *Opt. Express* **26**, 14307 (2018).
- W. Yang, X. Jin, X. Yu, *et al.*, *Opt. Express* **25**, 24262 (2017).
- M. Stefszky, C. Mow-Lowry, S. Chua, *et al.*, *Classical Quantum Gravity* **29**, 145015 (2012).
- P. Kwee, B. Willke, and K. Danzmann, *Appl. Phys. B* **102**, 515 (2011).
- M. T. Nery, J. R. Venneberg, N. Aggarwal, *et al.*, *Opt. Lett.* **3**, 677 (2021).
- H. Vahlbruch, D. Wilken, M. Mehmet, *et al.*, *Phys. Rev. Lett.* **121**, 173601 (2018).
- A. El Amili and M. Alouini, *Opt. Lett.* **40**, 1149 (2015).
- T. Cullen, S. Aronson, R. Pagano, *et al.*, *Opt. Lett.* **47**, 2746 (2022).
- J. Yu, Y. Qin, Z. Yan, *et al.*, *Opt. Express* **27**, 3247 (2019).
- B. Willke, N. Uehara, E. Gustafson, *et al.*, *Opt. Lett.* **23**, 1704 (1998).
- C. Li, S. Xu, Y. Xiao, *et al.*, *J. Opt.* **17**, 075802 (2015).
- C. Li, S. Xu, X. Huang, *et al.*, *Opt. Lett.* **40**, 1964 (2015).
- N. Jiao, R. Li, Y. Wang, *et al.*, *Opt. Laser Technol.* **154**, 108303 (2022).
- Q. Zhao, S. Xu, K. Zhou, *et al.*, *Opt. Lett.* **41**, 1333 (2016).
- A. Khalaidovski, A. Thüring, H. Rehbein, *et al.*, *Phys. Rev. A* **80**, 053801 (2009).
- H. Ritsch, P. Zoller, C. Gardiner, *et al.*, *Phys. Rev. A* **44**, 3361 (1991).
- T. Ralph and C. Savage, *Phys. Rev. A* **44**, 7809 (1991).
- H. Ritsch and P. Zoller, *Phys. Rev. A* **45**, 1881 (1992).
- T. Ralph and C. Savage, *J. Opt. Soc. Am. B* **9**, 1895 (1992).
- K. Gheri and D. Walls, *Phys. Rev. Lett.* **68**, 3428 (1992).
- E. Hanamura, Y. Kawabe, and A. Yamanaka, in *Quantum Nonlinear Optics* (Springer Science & Business Media, 2007).
- R. Paschotta, M. Collett, P. Kürz, *et al.*, *Phys. Rev. Lett.* **72**, 3807 (1994).
- M. J. Lawrence, R. L. Byer, M. Fejer, *et al.*, *J. Opt. Soc. Am. B* **19**, 1592 (2002).
- Z. Li, W. Ma, W. Yang, *et al.*, *Opt. Lett.* **41**, 3331 (2016).
- W. Zhang, J. Wang, Y. Zheng, *et al.*, *Appl. Phys. Lett.* **115**, 171103 (2019).
- S. Shi, Y. Wang, W. Yang, *et al.*, *Opt. Lett.* **43**, 5411 (2018).